Nanoscale

Accepted Manuscript

This article can be cited before page numbers have been issued, to do this please use: J. Huang, X. Pan, X. Liao, M. Yan, B. Dunn, W. Luo and L. Mai, *Nanoscale*, 2020, DOI: 10.1039/D0NR02161J.

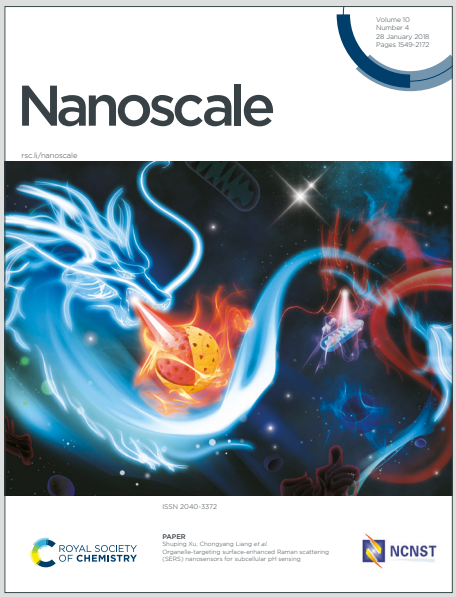

ROYAL SOCIETY OF CHEMISTRY

rsc.li/nanoscale

View Article Online
DOI: 10.1039/D0NR02161J

ARTICLE

In situ monitoring the electrochemically induced phase transition of thermodynamic metastable 1T-MoS_2 at nanoscale†

Received 00th January 20xx,
Accepted 00th January 20xx

DOI: 10.1039/x0xx00000x

Junxiao Huang [a], Xuelei Pan [a], Xiaobin Liao [a], Mengyu Yan [b], Bruce Dunn [c], Wen Luo*[ad], Liqiang Mai*[a]

1T-MoS_2 is widely used in hydrogen evolution reaction (HER) due to its abundant active sites and good conductivity. While 1T-MoS_2 is thermodynamically metastable due to the distorted crystal structure. Recently researchers have detected J_1 and A_{1g} Raman peaks after the HER process and confirmed that the 2H-1T phase possesses good stability. Therefore, the continuous HER is likely to transform the 1T-MoS_2 into a stable 2H-1T mixed phase.The in-situ characterization of 1T-MoS_2 individual nanosheet in HER process is important to understand intrinsic electrocatalytic behaviour at confined nanoscale, however which has rarely been investigated. Herein, we built an individual 1T-MoS_2 nanosheet micro-nano device by N-butyllithium intercalation into 2H-MoS_2.Then the device was kept at an overpotential (η= 450 mV) which is much lower than onset potential for 20 minutes to ensure continuous HER. Through this electrochemical treatment, we successfully obtained a mixed phase of 2H-1T and monitored the electrochemical phase transition by in situ Raman mapping and atomic force microscopy (AFM).The HER performance of the 2H-1T phase is superior to 1T-MoS_2 and 2H-MoS_2 。 Additionally, computational simulations demonstrate the 2H-1T phase exhibits optimal hydrogen adsorption energy. The presented work displays the intensive catalysis activity of the mixed phase obtained by electrochemical phase transition, which provides new directions for improving the catalytic activity of TMDs.

Introduction

Hydrogen is regarded as clean energy with the most development potential in the 21st century due to the advantages of high energy density, high fuel calorific value, and clean combustion products.[1] Electrochemical hydrogen evolution reaction (HER) is recognized as an efficient way to obtain hydrogen at present. Although platinum (Pt) and other precious metals have displayed excellent HER performance, replacing these expensive and rare materials with abundant non-noble metals to make HER more economic and efficient is still a hot topic of research today.[2-4] Recently, transition metal dichalcogenides (TMDs) have attracted attention in electrochemical community due to their layered structure, atomic level thickness, sufficient exposed active sites, low cost and large storage, and thus are considered as the most promising non-noble catalyst to surpass Pt.[5-10]

As a crucial material of TMDs, MoS_2 has been proven to have outstanding HER performance due to moderate hydrogen adsorption energy.[11-15] According to the coordination mode between the sulfur (S) atom and molybdenum (Mo) atom, MoS_2 presents in several polymorphs including 3R, 2H and 1T phases.[16-18] The 1T phase and the 2H phase are interchangeable, but the transition is not completely reversible. The MoS_2 of 2H phase or 1T phase can be synthesized directly by chemical vapor deposition (CVD),[18-21] and the 2H phase can be transformed into 1T phase by inserting macromolecular or alkali metal ions through chemical or electrochemical methods.[22-25] Unfortunately, the 1T phase is thermodynamically metastable due to the distorted crystal structure.[26-28] Therefore, it is easy to drive the transition from 1T phase to 2H phase by annealing, laser irradiation and electrochemical delithiation.[18, 29, 30] The bulk MoS_2 presents a plateau at ~1.1 V vs. Li/Li^+ during a discharge process.[30] This plateau is due to the lattice distortion caused by the intercalation of lithium ions into the MoS_2 layer, which transforms the 2H-MoS_2 into 1T phase. On the contrary, when the potential rises above 1.1 V vs. Li/Li^+, the 1T phase of MoS_2 will transform to the original 2H phase accompanying with the delithiation.

The excellent HER performance of 1T-MoS_2 has been reported in most researches, which can be attributed to the high conductivity and the active basal plane.[31, 32] However, the stability of the 1T-MoS_2 under the electrochemical condition is not clear. Most researches have only detected the presence of 1T phase after electrochemical process, but it is unclear whether a phase transition occurs during the electrochemical process and whether the product is 1T phase or mixed phase of 1T and 2H. Innovatively, the phase boundary of building 2H-1T

a. State Key Laboratory of Advanced Technology for Materials Synthesis and Processing, Wuhan University of Technology, Wuhan 430070, China
b. Materials Science and Engineering Department, University of Washington, Seattle, Washington 98195-2120, United States
c. Materials Science and Engineering, University of California, Los Angeles, California 90096, United States
d. Department of Physics, School of Science, Wuhan University of Technology, Wuhan 430070, China
Email: luowen_1991@whut.edu.cn ; mlq518@whut.edu.cn
† Electronic Supplementary Information (ESI) available: X-ray diffraction, and morphological characterization. See DOI: 10.1039/x0xx00000x

and domain boundary of 2H-2H have recently been proposed to significantly improve the HER performance of MoS_2 and explained the stability of 2H-1T phase.[33, 34] However, the aforementioned work only focused on the characterization of macro catalyst aggregate, and there is no effective means to operando measure specific materials or regions at nanoscale. Hence, it is significant to use a monolithic device-based platform to not only in-situ characterize an individual nanosheet during the electrochemical process but also detect each phase.

Here, we built an individual 1T-MoS_2 nanosheet micro-nano device by N-butyllithium intercalation into 2H-MoS_2. Then the device was kept at an overpotential (η= 450 mV) which is much lower than onset potential for 20 minutes to ensure continuous HER. This overpotential (– 0.45 V vs. NHE, at pH = 0) is equivalent to a potential of 2.59 V vs. Li/Li^+,[35] which is much higher than 1.1 V vs. Li/Li^+. So it is conducive to the spontaneous transition of the 1T phase to the 2H phase. Through this electrochemical treatment, we successfully obtained a stable mixed phase of 2H-1T. Raman mapping and atomic force microscopy (AFM) reveal phase transition and surface morphology changes of a fixed area in an individual MoS_2. The final 2H-1T phase MoS_2 after electrochemical treatment possesses a superior HER performance to those of 2H and 1T. The theory calculation demonstrates that the mechanism for the performance improvement is the boundary of the 2H-1T phase possesses more favorable ΔG_{H^*} for HER compared with the 2H and 1T phase.

Experimental Section

Fabrication of the individual 2H-MoS_2 nanosheet electrochemical device

A suitable sized silicon wafer substrate (with a 300-nm-thick insulation layer) was cut using a silicon knife and ultrasonically cleaned with acetone. The LOR3A and S1805 photoresists were spin-coated on silicon wafers at 3000 rpm for 40 s and the prepared silicon wafers were baked at 180 ℃ for 5 minutes. Then the device was patterned by ultraviolet lithography for 1.5s and deposited a certain thickness of Ti (5nm) and Au (25nm) by physical vapor deposition (PVD) to obtain the outer electrodes. The multilayered MoS_2 flakes were obtained from the bulk MoS_2 (single crystal) by mechanical exfoliation method[36] with Scott-tape. The as-exfoliated MoS_2 nanosheets were transferred to pre-patterned Si/SiO_2 substrate with Ti/Au (5 nm/25 nm) outer electrodes. Methyl Methacrylate (MMA) and Poly Methyl Methacrylate (PMMA) photoresists were spin-coated on the devices at 500 rpm for 10 s and 4000 rpm for 40 s, respectively. The devices were baked at 180 ℃ for 5 minutes or 60 ℃ for 500 s. E-beam lithography (EBL) and PVD were used to obtain Ti/Au (5 nm/80 nm) inner electrodes which connect the MoS_2 nanosheets to the outer electrodes. Finally, PMMA was used as insulating layer to prevent the electrolyte from contacting metal electrodes, and rectangular windows were opened by EBL. One electrode was connected to only one MoS_2 nanosheet to ensure that each MoS_2 was accurately measured.

Fabrication of the individual 1T-MoS_2 nanosheet electrochemical device

The individual 1T-MoS_2 nanosheet electrochemical device was obtained by the lithiation of 2H-MoS_2. In an argon atmosphere glove box, the prepared 2H-MoS_2 nanosheet electrochemical device was immersed in 1.6 M n-butyl lithium solution (Aladdin) for 6 hours. After intercalation, the samples were immersed respectively with hexane and deionized (DI) water for 1 minute and 2 minutes in the glove box to remove organic residues.

Fabrication of the individual 2H-1T-MoS_2 nanosheet electrochemical device

The 1T-MoS_2 nanosheet device was kept at an overpotential (η= 450 mV) which is much lower than onset potential of HER for 20 minutes to ensure continuous HER. After the electrochemical treatment, the 2H-1T-MoS_2 nanosheet electrochemical device was obtained.

Material and device characterization

JEOL JSM-7001F microscope and energy dispersive spectroscopy system (INCA X/MAX 250) were used to record the SEM images and the elemental mapping of the micro-nano devices at an acceleration voltage of 20 kV, respectively. The structural phases of the samples were characterized by XRD (Bruker D8 Advanced X-ray diffractometer with Cu-Kα radiation). The Autolab 302N and probe station (Lake Shore, TTPX) were combined to measure the electrical performance of the device. The electrochemical performances of the device were recorded by semiconductor device analyzer (Agilent B1500A).

Electrochemical measurement

A three-electrode system was used to electrochemically measure the device, the counter electrode was a graphite rod, the reference electrodes was saturated calomel electrode (SCE), and the working electrode was the MoS_2 nanosheet. The electrolyte was 0.5 M H_2SO_4. The 2H, 1T and mixed 2H-1T MoS_2 nanosheet devices were tested by immersed in a drop of 0.5 M H_2SO_4. The electrochemical treatment is to apply 450 mV overpotential to the 1T-MoS_2 for 20 minutes to ensure the continuous HER. The working electrode on the device is connected to the electrochemical workstation or the semiconductor analyzer through a probe station to complete subsequent performance tests. The conductivity characteristics of the individual nanosheet was measured by the semiconductor device analyzer combined with the probe station. The HER performance of MoS_2 nanosheet under different states was tested by combining Autolab 302N electrochemical workstation with the probe station. The linear sweep voltammetry was used to obtain the HER polarization curve, the scan rate was 5 mV s^{-1}.

Raman mapping and quasi in situ AFM measurement

After the photoresists were removed from the substrate, scanning probe microscopy (AIST-NT SPM) was used to obtain the atomic force microscopy (AFM) image. The Raman spectra were collected using a Horiba Scientific LabRAM HR evolution Raman spectrometer. In this section, the device was transferred and placed under the instrument after each-step treatment to ensure quasi in situ AFM measurement. The microscope on the instrument can accurately locate the device. The same size text box was selected for every time. The sample was tested under a laser with a power less than 0.1 mW and a wavelength of 532 nm to prevent a phase transition during the test.

DFT calculation

The present calculations were carried out by using the projector augmented wave (PAW) method within DFT, as implemented in the VASP. The generalized gradient approximation (GGA) in the form of the Perdew-Burke-Ernzerhof (PBE) was used to treat the exchange-correlation energy. A kinetic energy cut-off of 450 eV was used for wave functions expanded in the plane wave basis. Grimme method of method was used for describing the van der Waals interaction between the substrate. All atoms were allowed to relax until the forces were less than 0.03 eV $Å^{-1}$. For the Brillouin-zone sampling, 5*5*1 k-points were adopted to ensure convergence of the total energy. Monolayered MoS_2 crystal models with 10 Å vacuum layer were constructed for the H abortion simulation. The lattice parameters of the 1T and 2H phase were 9.66*9.66*18.17 and 9.57*9.57*23.13 Å, respectively. MoS_2 with 2H-1T phase boundary was carried out to investigate the catalytic activity of the phase boundary.

Results and Discussion

In this work, we obtained MoS_2 flakes from the bulk MoS_2 (single crystal) by mechanical exfoliation method[36] with Scott-tape. And the micro-nano devices were assembled by many steps subsequently (See Fig S1 and experimental section for more details). The XRD, SEM and EDX (Energy-dispersive X-ray spectroscopy) patterns of bulk MoS_2 and the device are shown in Fig S2. Fig 1a shows a schematic of the individual MoS_2 nanosheet electrocatalytic device. Based on the nanodevice with a three-electrode system, we performed a continuous electrochemical treatment on the nanosheets after lithiation, which was shown on the upper side of Fig 1b. The 1T-MoS_2 nanosheet device was kept at an overpotential (η= 450 mV) which is much lower than onset potential of HER for 20 minutes to ensure continuous HER,[12, 18, 31] and the current density of the device is continuously increases. The electrode potential to drive HER of 1T-MoS_2 is favorable to the phase transition back to 2H phase. Therefore, the 2H-1T mixed phase of MoS_2 was obtained after such an electrochemical treatment. Chronopotentiometric stability test after all the following electrochemical and electrical tests was conducted to explore the catalytic stability of the 2H-1T MoS_2, which was shown on the lower side of Fig 1b. The current density of the 2H-1T MoS_2 was relatively stable compared with the top of Fig 1b, which demonstrates that the final product obtained by electrochemical treatment possesses a particularly stable phase. Raman spectra of final product at different time were shown in Fig S3.

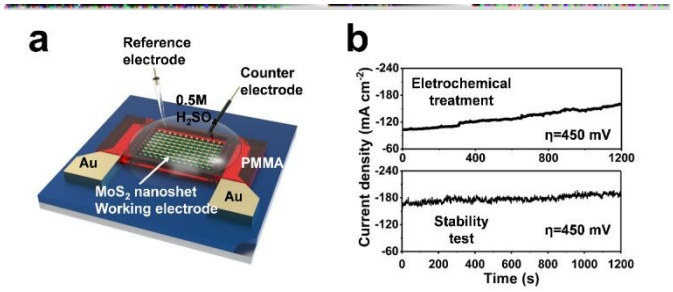

Fig. 1 (a) Schematic of the individual MoS_2 nanosheet-based electrocatalytic nanodevice. (b) The upper one is the electrochemical treatment: chronopotentiometric test curve and the overpotential is 450 mV applied on 1T-MoS_2 device to ensure continuous HER, the lower one is the post-chronopotentiometric stability test at a constant overpotential of 450 mV applied on the 2H-1T-MoS_2 device after all the following electrochemical and electrical tests.

Then we prepared three states of samples to investigate the electrochemical phase transition. Typically, the state Ⅰ is the initial 2H phase, the state Ⅱ is the metastable 1T phase of MoS_2 lithiated by n-butyllithium, and the state Ⅲ is the 2H-1T phase of MoS_2 after electrochemical treatment. Polarization curves of three states are shown in Fig 2a, and the Tafel slopes in Fig 2b. The results indicate that the overpotential of the state Ⅰ is 292.5 mV at 10 mA cm^{-2}, and Tafel slope is 328.3 mV dec^{-1}, which shows a moderate HER performance. The state Ⅱ displays a lower overpotential of 209.4 mV at 10 mA cm^{-2}, 169.1 mV dec^{-1}. The performance improvement is due to the phase transition occurs after intercalating Li ions, obviously. And the state Ⅲ shows an enhanced electrochemical activity, the overpotential is 194.8 mV at 10 mA cm^{-2} with a Tafel slope of 113.1 mV dec^{-1}, which is coincide with the recent work.[34] The enhanced performance is due to that the metastable 1T-MoS_2 nanosheet transforms to a mixed phase after the electrochemical reaction. Afterwards, I-V measurement reveals the conductivity of the three states in Fig 2c. It is found from Fig 2f that the conductivity of state Ⅰ is only 6.32 S m^{-1}. When phase transition occurs after lithiation, the conductivity increases to 678.46 S m^{-1} significantly because the 2H phase is a semiconductive phase, and the 1T phase is a metallic phase.[24, 29, 31] The conductivity of the state Ⅲ decreases to 502.4 S m^{-1} since the partial 1T phase is reduced to the 2H phase, forming a mixed phase after the continuous electrochemical treatment. Besides, electrochemical impedance spectroscopy (EIS) test was carried out to investigate the electrode kinetics under HER conditions.[37, 38] The Nyquist plots are shown in Fig 2d and the specific values of R_{ct} are shown in Fig 2g. The state Ⅰ displays a much larger impedance in the complex plane and the state Ⅲ displays the smallest impedance. These results demonstrate that the state Ⅲ shows best charge transfer rate. Furthermore, it is interesting that state Ⅲ shows a different plot in Fig 2e, the bode plots show one more hump at high-frequency region. Hence, the Nyquist plot is considered as three part of arcs corresponding to a three-time constant model. This can be

View Article Online
DOI: 10.1039/D0NR02161J

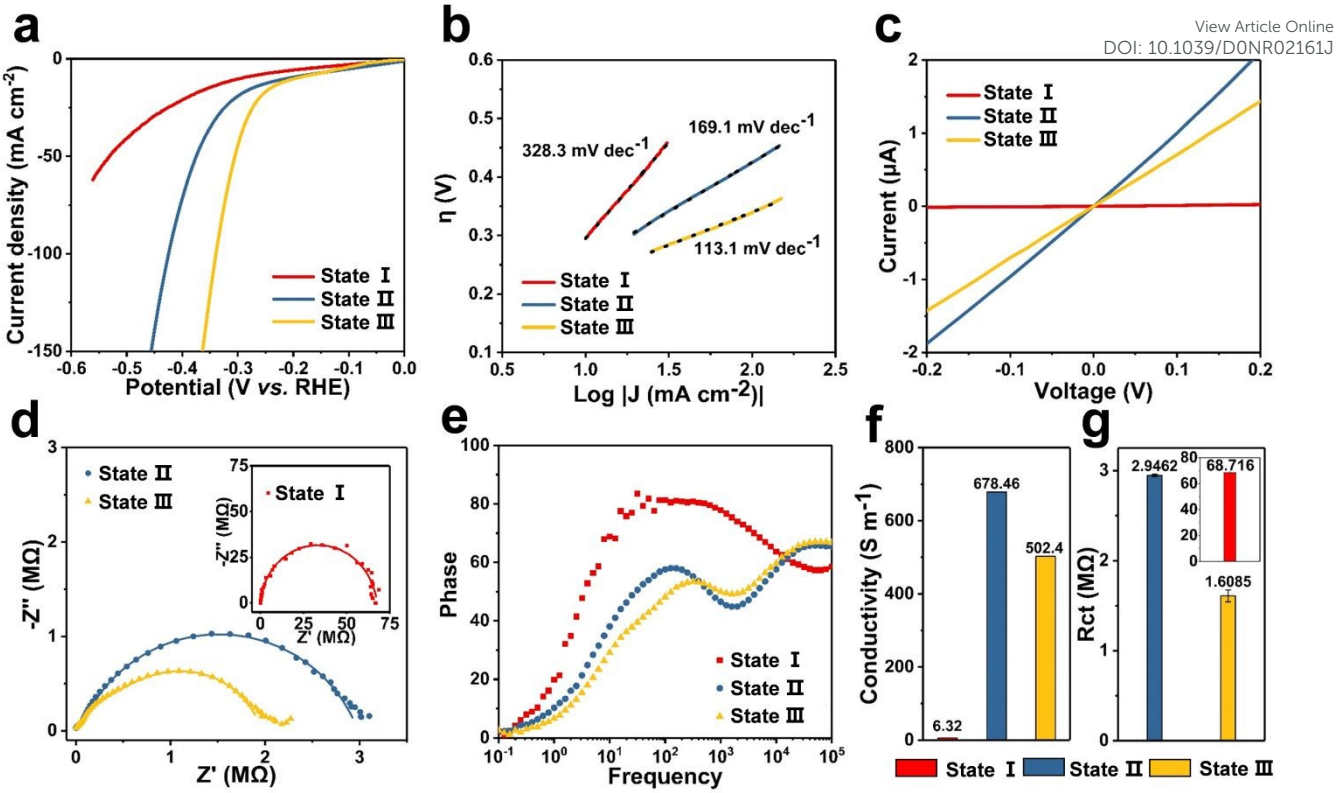

Fig. 2 The performance of the three states (the state Ⅰ is the initial 2H phase, the state Ⅱ is the metastable 1T phase of MoS_2 lithiated by n-butyllithium, and the state Ⅲ is the 2H-1T phase of MoS_2 after electrochemical treatment). (a) The polarization curves. (b) The corresponding Tafel slopes. (c) I-V curves. (d) Impedance measurements: Nyquist plots. (e) Bode plots. (f) The specific conductivity corresponding to (c). (g) The specific simulation R_{ct} values corresponding to (d).

attributed to the mixed phase in state Ⅲ and the induced quantum capacitance of mixed phase of MoS_2.[39-41] In addition, as shown in the Fig S3b and S3c, we performed other seven sets of the same repetitive experiments. The same electrochemical treatment was applied to 1T-MoS_2 and gathered the statistic data of corresponding specific overpotentials at current densities of 50 mA cm^{-2} and 100 mA cm^{-2}. The statistical graph shows that under different current density conditions, the overpotential of the state Ⅲ is always smaller than that of the 2H and 1T. This shows that the state Ⅲ does have better electrochemical performance than the state Ⅰ and state Ⅱ.

The optical images of the three states are shown in Fig 3a and Fig 3d, with the inset shows the state Ⅰ of the device. In the initial state Ⅰ, the part of the MoS_2, exposed in a window etched by the electron beam is very smooth and flat. After lithiation, the exposed part in the middle becomes dark black, which indicates that the intercalation reaction occurs in the exposed area, consistent with the previous report.[23] Finally, after the continuous electrochemical treatment, the intermediate part returns to light black, indicating that the electrochemical treatment has a tendency to restore the surface state of MoS_2 from the state Ⅱ to the initial state Ⅰ. For two-dimensional materials such as MoS_2, Raman spectroscopy is recognized as a primary characterization method to distinguish the structure of different phases caused by representative vibration modes. To investigate the phase transition process of MoS_2 nanosheet, in situ Raman characterization was performed. Two types of in situ Raman mapping (peak intensity and peak position) have monitored all the phase transitions. The peak intensity Raman mapping is shown in Fig 3b and 3e. The peak position Raman mapping is shown in Fig S4. The Raman spectra of 2H phase MoS_2 have two important modes of vibration, E_{2g} (in plane optical vibration of the Mo-S bond with the S atoms and the Mo atoms vibrate in opposite directions) and A_{1g} modes (out of plane optical vibration of S atoms) which are located at 383 cm^{-1}, 409 cm^{-1}, respectively.[23, 42] The Raman spectra of 1T phase have three additional modes of vibration in addition to E_{2g} and A_{1g} of 2H phase: J_1 (156 cm^{-1}), J_2 (226 cm^{-1}) and J_3 (333 cm^{-1}). When 2H phase transforms to 1T phase, the E_{2g} mode and A_{1g} mode weaken gradually, and the generation of three new modes is attributed to the distorted superlattice structure of 1T phase. The recent works have shown that in 1T phase MoS_2 Raman specta, J_1 mode is the in-plane shear mode, J_2 mode is related to the slip of sulfur atom layer relative to molybdenum atom, and J_3 mode reflects the elongation of one side of the zigzag chains relative to the other side.[26-28, 42] Since J_1 peak is the most obvious in 1T phase, A_{1g} peak is the most representative in 2H phase. Therefore, for the peak intensity Raman mapping, we choose two main Raman shift ranges (150~160 cm^{-1} and 405~415 cm^{-1}, with only J_1 and A_{1g} peaks are in these two ranges

View Article Online
DOI: 10.1039/D0NR02161J

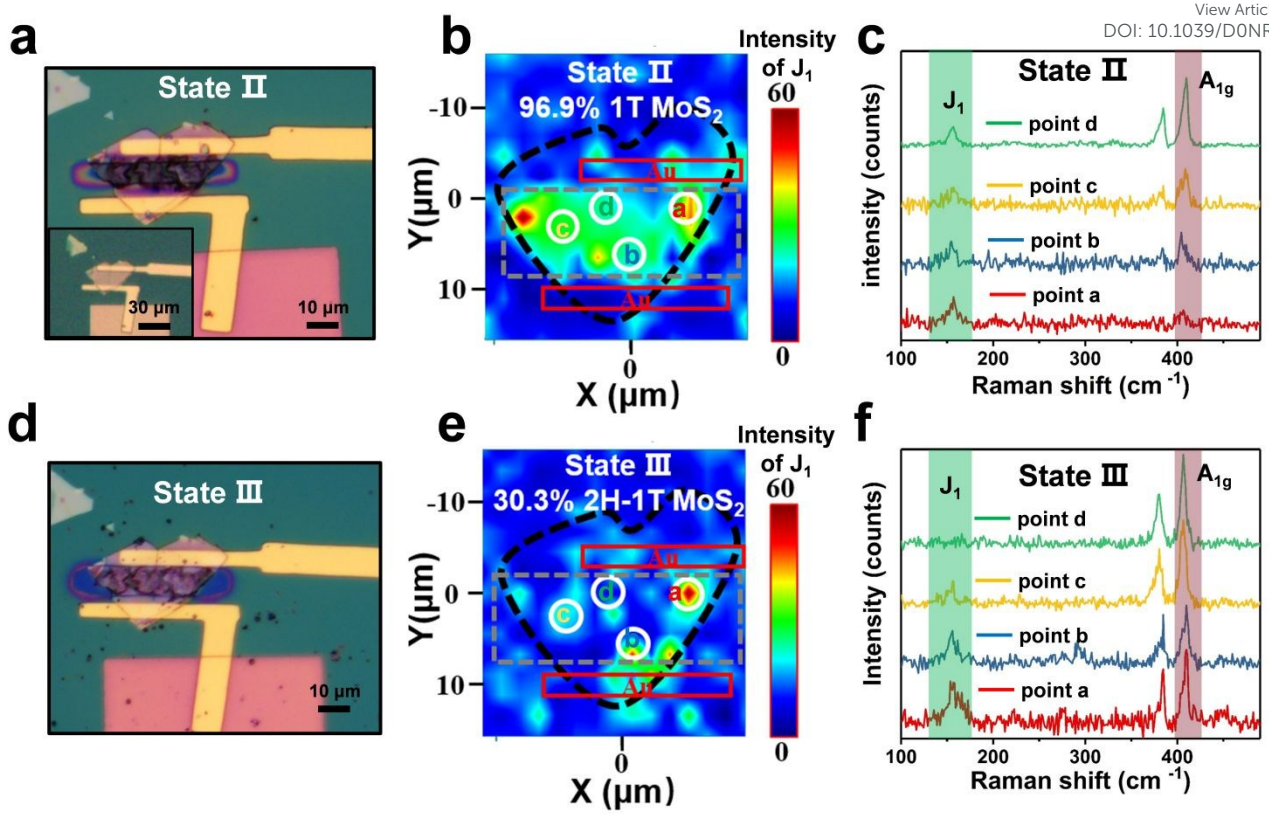

Fig. 3 The in situ Raman mapping of the device. (a) Optical microscope image of the state Ⅱ. (The illustration in the left bottom corner in this image is the optical micrograph of the state Ⅰ.) (b) Raman mapping of the J_1 peak under state Ⅱ, the area with high J_1 peak intensity accounts for 96.9 % of the total area. (c) The specific Raman spectra of the fixed point (point a, b, c and d) corresponding to the Raman mapping in (b), and the intensity ratio of A_{1g}/J_1 at each point is low. (d) Optical microscope image of the state Ⅲ. (e) Raman mapping of the J_1 peak under state Ⅲ, the area with high J_1 peak intensity accounts for 30.3 % of the total area. (f) The specific Raman spectra of the fixed point (point a, b, c and d) corresponding to the Raman mapping in (e), and the intensity ratio of A_{1g}/J_1 at each point is high.

respectively) to represent the phase transition. The Raman intensity mappings of J_1 peak are shown in Fig 3b and 3e. The Raman intensity mappings of A_{1g} peak are shown in Fig S5. As was seen from 3b and 3e, the black dashed line defines the contour of the MoS_2, the gray dashed line indicates the exposed region of the selective phase change and the red solid line represents the gold electrode. It can be seen from Fig 3b that in the selective exposed region, the peak intensity of J_1 peak (color in green) is strong. However, from the corresponding A_{1g} peak in Fig S5a, the intensity of the same region (color in blue) is very low. This indicates that most of the initial 2H-MoS_2 is transformed to 1T-MoS_2 after lithiation. The ratio of phase transition can be obtained from Raman mapping. Since the green area accounts for about 96.9 % of the total area, it can be considered that 96.9 % of the 1T-MoS_2 was finally formed. Subsequently, as shown in Fig 3e, in the same area compared with Fig 3b, most of the green disappears into blue, which indicates the disappearance of the J_1 peak. Similarly, in Fig S5b, compared with S5a, most of the blue in the same area disappears into green, which indicates the appearance of the A_{1g} peak. These phenomena together indicate that the electrochemical treatment from state Ⅱ to state Ⅲ causes a phase transition of 1T-MoS_2. According to the above proportion calculation method, the green area in Fig 3e accounts for 30.3 % of the total area. It indicates that the final mixed phase formed is 2H-1T with the content of 30.3 %. All the results illustrate that electrochemical treatment can drive the phase transition of the 1T-MoS_2. Furthermore, we performed characterization of the four fixed individual points (colored red, blue, yellow and green selected in Fig 3c and Fig 3f) to accurately describe the electrochemical phase transition process. According to a spatially resolved Raman spectra of MoS_2, the intensity ratio of A_{1g} to J_1 peak can be used to determine the phase content. The value of A_{1g}/J_1 is inversely proportional to the content of 1T phase. As it can be seen from Fig 3c, the J_1 peak is obvious, and the value of A_{1g}/J_1 is relatively low, which indicates that the content of 1T phase is very high at this time. After the electrochemical treatment, as shown in Fig 3f, the J_1 peak at green point has disappeared, and the A_{1g} peak at all points has become apparent. The value of A_{1g}/J_1 increased relatively. This shows that the content of the 1T phase is decreasing and a mixed phase of 2H-1T has been formed. In

order to exclude the influence of electrolyte, a control experiment was conducted whereby the device was dipped in H_2SO_4 for 20 minutes. The results showed that there was no significant change in Raman mapping nor Raman spectra at fixed points before and after dipping (See Fig S4 for more details).

Since the process of phase transition is caused by the intercalation of n-butyllithium, with regard to the possible presence of lithium ions between the layers of MoS_2 which could not be characterized by Raman. [23, 32, 33, 43] In situ AFM test was conducted afterward. The phase of each MoS_2 has been identified before the AFM test. As shown in Fig 4, three different devices (Ⅰ, Ⅱ, Ⅲ) were prepared to monitor the surface morphology changes of MoS_2 obtained by two different treatment (A and B) methods. The device Ⅱ is our experimental group, the corresponding device Ⅰ and device Ⅲ are our control groups. Treatment A is the electrochemical treatment, and the treatment B only dips the device in H_2SO_4 solution for 20 minutes. It was found from Fig 4a, 4b and 4c that the surface of MoS_2 in the state Ⅰ is very smooth and flat. However, it was found from Fig 4d, 4e and Fig S6b that after the lithiation, the phase transition to 1T phase occurs, the surface exposed by electron beam appears 'bubble' like morphology and the area covered by PMMA is bulging. This is due to the intercalation of lithium ions into the layers of MoS_2, which enlarges the interlayer spacing and increases the stress between the layers. Besides, as shown in equation (1) and (2), the reaction of n-butyl lithium with 2H-MoS_2 results in the formation of Li_xMoS_2. The subsequent immersion in deionized water caused the reaction of the Li_xMoS_2 with the water molecules to produce a large amount of H_2. The H_2 released from the surface of MoS_2, resulting in 'bubble' phenomenon. It can be found in Fig 4g that the surface recovers to a relatively flat state, and the bulged area disappears after the treatment B for device Ⅰ. However, the sample still maintains the 1T phase. After the treatment A for device Ⅱ, as shown in Fig 4h, the surface becomes relatively flat while the bulged area completely disappears, and the phase transition occurs at the same time. Combined with Raman results, it is shown that under the electrochemical treatment, lithium ions in 1T-MoS_2 will be de-intercalated to form a mixed phase of 2H-1T, so the surface morphology will change. Even as result of the HER is too intense, some samples have cracks or even folds on the surface (See Fig S6 for more details). Fig S7a

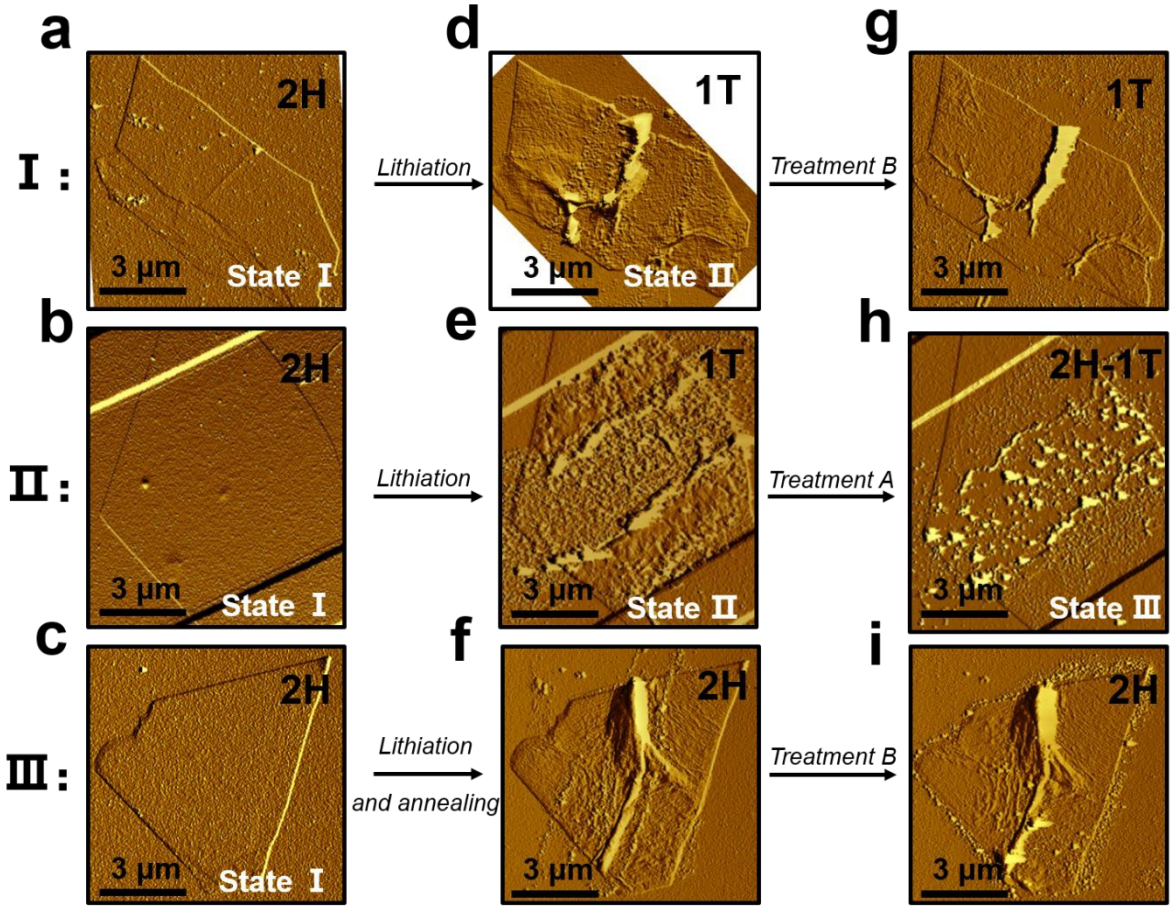

Fig. 4 The quasi AFM image of three different devices of MoS_2. The phase of each MoS_2 has been identified before the AFM test. Treatment A: the electrochemical treatment; Treatment B: only dipping the device in H_2SO_4 solution for 20 minutes. (a) (b) (c) The initial state of 2H-MoS_2 correspond to device Ⅰ, Ⅱ and Ⅲ. (d) (e) 1T-MoS_2 after lithiation correspond to (a) and (b). (f) Fully annealing to 2H-MoS_2 after lithiation correspond to (c). (g) Treatment B for device Ⅰ. (h) Treatment A for device Ⅱ. (i) Treatment B for device Ⅲ

shows the thickness of the device Ⅱ in Fig 4b is 11.72 nm, the Fig 4e is 46.91nm, and the Fig 4h is 20.59 nm. As shown in Fig 4f, after the device is completely annealed from the 1T phase to the 2H phase, there is no significant surface changes compared to Fig S7b. After the treatment B for device Ⅲ, the surface of the device has a certain recovery tendency as shown in Fig 4i, but the degree of recovery is far less than the final device Ⅱ. From the above three sets of experiments, we can draw the following conclusions: lithium ions will be de-intercalated from the interlayer of MoS_2 under the atmosphere of H_2SO_4, resulting in the disappearance of stress, so that the surface of MoS_2 has a recovery trend. It was seen from the annealing phase transition process that the phase change can make the surface have a certain recovery ability. However, the electrochemical treatment will accelerate the surface recovery rate due to the extraction of lithium ions, thereby transforming the 1T-MoS_2 to the mixed 2H-1T phase.

$$x\ C_4H_9Li + MoS_2 \rightarrow Li_xMoS_2 + x/2\ C_8H_{18}\ (1)$$

$$Li_xMoS_2 + x\ H_2O \rightarrow x\ LiOH + MoS_2 + x/2\ H_2\uparrow\ (2)$$

First-principles calculations based on density functional theory (DFT) were performed to further investigate the source of catalytic activities of the three states (See experimental section for more details). Fig 5a shows the optimized structures of three states with adsorbed protons. It was found that in the 2H and 1T phases of MoS_2, protons are adsorbed on the surface of sulfur atoms. And in the 2H-1T mixed phase, the protons are adsorbed at the boundary, which indicates that the adsorption energy at the boundary of 2H-1T is lower, and the combination with protons is easier than the 2H and 1T phases. The electronegativity of the three states are shown in Fig S8, and whether it is a sulfur atom or a molybdenum atom, the electronegativity at the 2H-1T boundary is higher than that of 2H and 1T. Fig 5b shows the calculated Gibbs free energy of the adsorbed atomic hydrogen (ΔG_{H^*}). As a widely accepted indicator of catalytic activity, the optimum value for catalytic activity is ΔG_{H^*} = 0 eV, which deliver neither too strong nor too weak interaction for hydrogen absorption and release.[44] We performed the calculations on the basal plane of the 2H, 1T and 2H-1T phase with the same sized cells and Pt (1 1 1) surface used for comparison, yielding ΔG_{H^*} = 1.77 eV, 0.34 eV, 0.21 eV, -0.18 eV. The results indicate that the pure 2H and 1T phases show moderate adsorption of hydrogen atoms which perform relatively week binding energy for hydrogen.[34, 45, 46] Remarkable, the 2H-1T phase exhibits optimal hydrogen adsorption energy, indicating that the mixed structure can improve the combination between the H atom and the adsorption sites.

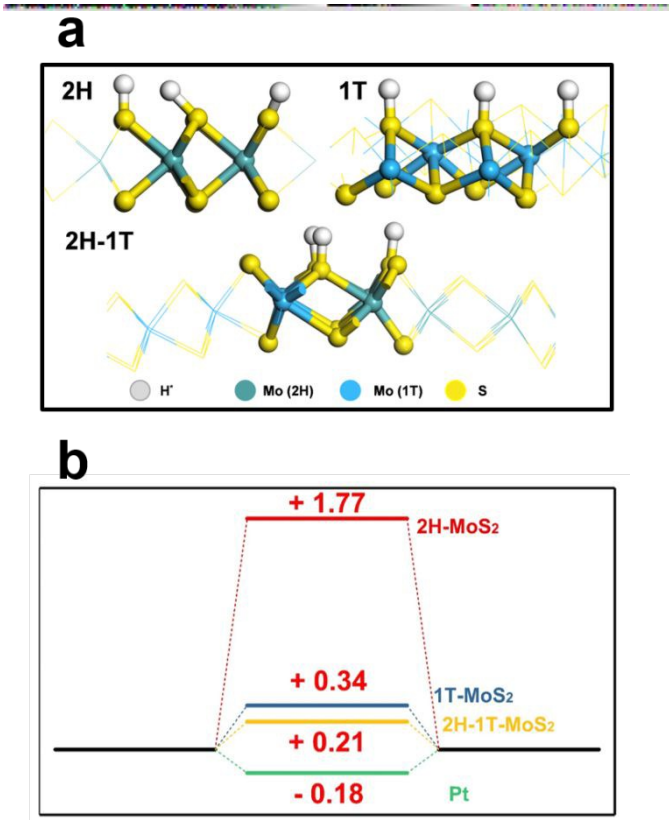

Fig. 5 First-principles calculations based on DFT of the three states. (a) Computational simulation diagram of three states adsorbing three protons. (b) Gibbs free energy of the adsorbed atomic hydrogen curves.

Conclusions

In conclusion, a 2H-1T mixed phase of MoS_2 nano-device with satisfactory HER performance (194.8 mV at 10 mA cm^{-2}, 113.1 mV dec^{-1}) was successfully obtained by a novel and mild electrochemical treatment whereby the 1T-MoS_2 device was kept at an overpotential (η= 450 mV) to ensure continuous HER. And then Raman and AFM were combined to in situ monitor the phase transition process at nanoscale. Based on the observed phenomena, it was concluded by theoretical calculations that the reason for improving HER performance is due to the boundary of the 2H-1T phase possesses more favorable ΔG_{H^*} for HER compared with the 2H and 1T phase. These results show the mixed phase of 2H-1T obtained by electrochemical treatment has an excellent HER performance, which will provide new directions for improving the catalytic activity of TMDs.

Conflicts of interest

There are no conflicts to declare.

Acknowledgements

This word was supported by the National Natural Science Fund for Distinguished Yong Scholars (51425204), the National Science Foundation of China (51904216, 51832004, 51521001), the National Key R & D Program of China (2016YFA0202603), the Yellow Crane Talent (Science & Technology) Program of

Wuhan City, the International Science & Technology Cooperation Program of China (2013DFA50840), National Basic Research Program of China (2013CB934103), the Fundamental Research Funds for the Central Universities (WUT: 2017-YB-005).

References

1. Thoi, V. S.; Sun, Y.; Long, J. R.; Chang, C. J., Chem. Soc. Rev. 2013, 42, 2388-2400.
2. Zhang, J.; Zhao, Y.; Guo, X.; Chen, C.; Dong, C.-L.; Liu, R.-S.; Han, C.-P.; Li, Y.; Gogotsi, Y.; Wang, G, Nat. Catal. 2018, 1, 985-992.
3. Zhuang, Z.; Li, Y.; Li, Z.; Lv, F.; Lang, Z.; Zhao, K.; Zhou, L.; Moskaleva, L.; Guo, S.; Mai, L., Angew. Chem. Int. Edit. 2018, 57, 496-500.
4. Ling, T.; Zhang, T.; Ge, B.; Han, L.; Zheng, L.; Lin, F.; Xu, Z.; Hu, W. B.; Du, X. W.; Davey, K., et al., Adv. Mater. 2019, 31, 1807771.
5. Er, D.; Ye, H.; Frey, N. C.; Kumar, H.; Lou, J.; Shenoy, V. B., Nano Lett. 2018, 18, 3943-3949.
6. Henckel, D. A.; Lenz, O. M.; Krishnan, K. M.; Cossairt, B. M., Nano Lett. 2018, 18, 2329-2335.
7. Nguyen, V. T.; Yang, T. Y.; Le, P. A.; Yen, P. J.; Chueh, Y. L.; Wei, K. H., ACS Appl. Mater. Inter. 2019, 11, 14786-14795.
8. Zhou, Y.; Pondick, J. V.; Silva, J. L.; Woods, J. M.; Hynek, D. J.; Matthews, G.; Shen, X.; Feng, Q.; Liu, W.; Lu, Z., et al., Small. 2019, 1900078.
9. Yan, M.; Zhou, X.; Pan, X.; Wang, J.; Xia, L.; Yu, K.; Liao, X.; Xu, X.; He, L.; Mai, L., Nano Res. 2018, 11, 3205-3212.
10. Yan, M.; Pan, X.; Wang, P.; Chen, F.; He, L.; Jiang, G.; Wang, J.; Liu, J. Z.; Xu, X.; Liao, X., et al., Nano Lett. 2017, 17, 4109-4115.
11. Voiry, D.; Yang, J.; Chhowalla, M., Adv. Mater. 2016, 28, 6197-6206.
12. Wang, J.; Yan, M.; Zhao, K.; Liao, X.; Wang, P.; Pan, X.; Yang, W.; Mai, L., Adv. Mater. 2017, 29, 1604464.
13. Gao, G.; Jiao, Y.; Ma, F.; Jiao, Y.; Waclawik, E.; Du, A., J. Phys. Chem. C. 2015, 119, 13124-13128.
14. Kan, M.; Wang, J. Y.; Li, X. W.; Zhang, S. H.; Li, Y. W.; Kawazoe, Y.; Sun, Q.; Jena, P., J. Phys. Chem. C. 2014, 118, 1515-1522.
15. Wang, H.; Tsai, C.; Kong, D.; Chan, K.; Abild-Pedersen, F.; Nørskov, J. K.; Cui, Y., Nano Res. 2015, 8, 566-575.
16. Voiry, D.; Mohite, A.; Chhowalla, M., Chem. Soc. Rev. 2015, 44, 2702-2712.
17. Fang, Y.; Pan, J.; He, J.; Luo, R.; Wang, D.; Che, X.; Bu, K.; Zhao, W.; Liu, P.; Mu, G., et al., Angew. Chem. Int. Edit. 2018, 57, 1232-1235.
18. Yu, Y.; Nam, G. H.; He, Q.; Wu, X. J.; Zhang, K.; Yang, Z.; Chen, J.; Ma, Q.; Zhao, M.; Liu, Z., et al., Nat. Chem. 2018, 10, 638–643.
19. Liu, L.; Wu, J.; Wu, L.; Ye, M.; Liu, X.; Wang, Q.; Hou, S.; Lu, P.; Sun, L.; Zheng, J., et al., Nat. Mater. 2018, 17, 1108–1114.
20. Sun, L.; Yan, X.; Zheng, J.; Yu, H.; Lu, Z.; Gao, S. P.; Liu, L.; Pan, X.; Wang, D.; Wang, Z., et al., Nano Lett. 2018, 18, 3435-3440.
21. Zhang, J.; Wu, J.; Guo, H.; Chen, W.; Yuan, J.; Martinez, U.; Gupta, G.; Mohite, A.; Ajayan, P. M.; Lou, J., Adv. Mater. 2017, 29, 1701955.
22. Wang, Q. H.; Kalantar-Zadeh, K.; Kis, A.; Coleman, J. N.; Strano, M. S., Nat. Nanotechnol. 2012, 7, 699-712.
23. Xiong, F.; Wang, H.; Liu, X.; Sun, J.; Brongersma, M.; Pop, E.; Cui, Y., Nano Lett. 2015, 15, 6777-6784.
24. Guo, Y.; Sun, D.; Ouyang, B.; Raja, A.; Song, J.; Heinz, T. F.; Brus, L. E., Nano Lett. 2015, 15, 5081-5088.
25. Huang, L.; Wei, Q.; Xu, X.; Shi, C.; Liu, X.; Zhou, L.; Mai, L., Phys. Chem. Chem. Phys. 2017, 19, 13696-13702.
26. Li, T., Rev. B. 2012, 85, 235407.
27. Jiménez Sandoval, S.; Yang, D.; Frindt, R. F.; Irwin, J. C., Phys. Rev. B. 1991, 44, 3955-3962.
28. Calandra, M., Phys. Rev. B. 2013, 88, 245428.
29. Tan, S. J. R.; Sarkar, S.; Zhao, X.; Luo, X.; Luo, Y. Z.; Poh, S. M.; Abdelwahab, I.; Zhou, W.; Venkatesan, T.; Chen, W., et al., ACS Nano. 2018, 12, 5051-5058.
30. Wang, H.; Lu, Z.; Xu, S.; Kong, D.; Cha, J. J.; Zheng, G.; Hsu, P. C.; Yan, K.; Bradshaw, D.; Prinz, F. B., et al., P. Natl. Acad. Sci. USA. 2013, 110, 19701-6.
31. Tan, C.; Luo, Z.; Chaturvedi, A.; Cai, Y.; Du, Y.; Gong, Y.; Huang, Y.; Lai, Z.; Zhang, X.; Zheng, L., et al., Adv. Mater. 2018, 30, 1705509.
32. Lin, Z.; Liu, Y.; Halim, U.; Ding, M.; Liu, Y.; Wang, Y.; Jia, C.; Chen, P.; Duan, X.; Wang, C., et al., Nature. 2018, 562, 254-258.
33. Ke, Q.; Zhang, X.; Zang, W.; Elshahawy, A. M.; Hu, Y.; He, Q.; Pennycook, S. J.; Cai, Y.; Wang, J., Small. 2019, 1900131.
34. Zhu, J.; Wang, Z.-C.; Dai, H.; Wang, Q.; Yang, R.; Yu, H.; Liao, M.; Zhang, J.; Chen, W.; Wei, Z., et al., Nat. Commun. 2019, 10, 1348.
35. Yang, C.; Rousse, G.; Louise Svane, K.; Pearce, P. E.; Abakumov, A. M.; Deschamps, M.; Cibin, G.; Chadwick, A. V.; Dalla Corte, D. A.; Anton Hansen, H., et al., Nat. Commun. 2020, 11, 1378.
36. Novoselov, K. S.; Geim, A. K.; Morozov, S. V.; Jiang, D., .; Zhang, Y., .; Dubonos, S. V.; Grigorieva, I. V.; Firsov, A. A., Science. 2004, 306, 666-669.
37. Wang, P.; Yan, M.; Meng, J.; Jiang, G.; Qu, L.; Pan, X.; Liu, J. Z.; Mai, L., Nat. Commun. 2017, 8, 645.
38. Watzele, S.; Fichtner, J.; Garlyyev, B.; Schwämmlein, J. N.; Bandarenka, A. S., ACS Catal. 2018, 8, 9456-9462.
39. Chen, X.; Wu, Z.; Xu, S.; Wang, L.; Huang, R.; Han, Y.; Ye, W.; Xiong, W.; Han, T.; Long, G., et al., Nat. Commun. 2015, 6, 6088.
40. Chu, L.; Schmidt, H.; Pu, J.; Wang, S.; Ozyilmaz, B.; Takenobu, T.; Eda, G., Sci. Rep. 2014, 4, 7293.
41. Xia, J.; Chen, F.; Li, J.; Tao, N., Nat. Nanotechnol. 2009, 4, 505-509.
42. Fan, J.-H.; Gao, P.; Zhang, A.-M.; Zhu, B.-R.; Zeng, H.-L.; Cui, X.-D.; He, R.; Zhang, Q.-M., J. Appl. Phys. 2014, 115, 053527.
43. Zhang, K.; Jin, B.; Gao, Y.; Zhang, S.; Shin, H.; Zeng, H.; Park, J. H., Small. 2019, 15, 1901883.
44. Jiao, Y.; Zheng, Y.; Jaroniec, M.; Qiao, S. Z., Chem. Soc. Rev. 2015, 44, 2060-2086.
45. Tang, Q.; Jiang, D.-e., ACS Catal. 2016, 6, 4953-4961.
46. Yin, Y.; Han, J.; Zhang, Y.; Zhang, X.; Xu, P.; Yuan, Q.; Samad, L.; Wang, X.; Wang, Y.; Zhang, Z., et al., J. Am. Chem. Soc. 2016, 138, 7965-7972.

DOI: 10.1039/D0NR02161J

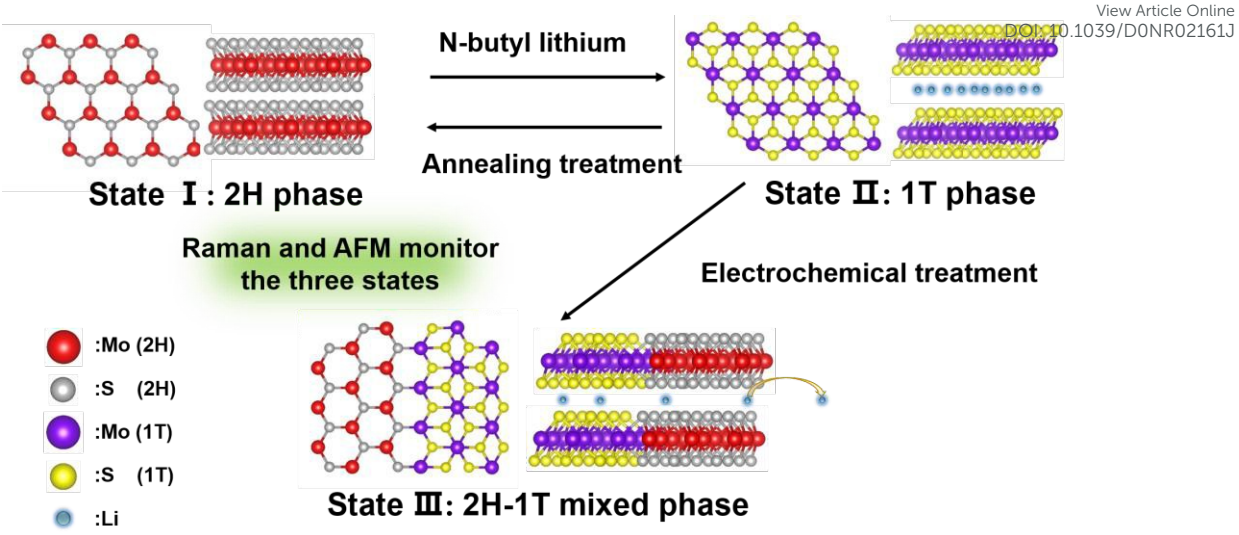

A new phase transition of 1T-MoS_2 during the electrochemical treatment was discovered and in situ monitored.